HOKKAIDO UNIVERSITY

Title	Synthesis of Mo1-xNbxS2 thin films by separate-flow chemical vapor deposition with chloride sources
Author(s)	Yanase, Takashi; Watanabe, Sho; Uehara, Fumiya; Weng, Mengting; Nagahama, Taro; Shimada, Toshihiro
Citation	Thin solid films, 649, 171-176 https://doi.org/10.1016/j.tsf.2018.01.052
Issue Date	2018-03-01
Doc URL	http://hdl.handle.net/2115/76823
Rights	© 2018. This manuscript version is made available under the CC-BY-NC-ND 4.0 license http://creativecommons.org/licenses/by-nc-nd/4.0/
Rights(URL)	https://creativecommons.org/licenses/by-nc-nd/4.0/
Type	article (author version)
File Information	revised manuscript_part2_ver.3.pdf

Instructions for use

Hokkaido University Collection of Scholarly and Academic Papers : HUSCAP

Title: Synthesis of $Mo_{1-x}Nb_xS_2$ thin films by separate-flow chemical vapor deposition with chloride sources

Takashi Yanase†*, Sho Watanabe†, Fumiya Uehara†, Weng Mengting†, Taro Nagahama†, Toshihiro Shimada†

† Division of Applied Chemistry, Faculty of Engineering, Hokkaido University, Kita 13 Nishi 8 Kita-ku, Sapporo 060-8628, Japan

*Corresponding author: Takashi Yanase

Email address: yanase42@eng.hokudai.ac.jp (T. Y.)

Abstract

The doping of element (Nb, Ta, etc.) into MoS_2, one of the layered transition metal dichalcogenides, is a key technology for electronic devices because the lack of the p-type MoS_2 has limited the range of applications. We report that the $Mo_{1-x}Nb_xS_2$ thin films were synthesized on SiO_2/Si substrates by chemical vapor deposition (CVD). It was critical to use chloride sources ($MoCl_5$ and $NbCl_5$) for the synthesis of $Mo_{1-x}Nb_xS_2$. The Nb concentration can be increased to 10% by controlling the supplied amount of Nb using a separate-flow CVD apparatus. The Raman spectra changed as the Nb concentration increased, appearing E_2(Nb-S) vibrational mode. The photoluminescence (PL) at 655 nm,

attributed to emission from excitons, disappeared, when Nb was incorporated into the MoS_2. PL due to trions at 680 nm was observed for the $Mo_{1-x}Nb_xS_2$ thin films.

Keywords

chemical vapor deposition, $Mo_{1-x}Nb_xS_2$, alloying

Introduction

Transition metal dichalcogenides (TMDCs), particularly MoS_2, were studied as catalysts, lubricants and substrates for heteroepitaxy from 1970s - 1990s [1-5]. The doping and alloying with several elements (Co, Au, Ni etc.) were conducted to improve their performance. However, MoS_2 did not gather researchers' attention as a semiconducting material at that time.

The study of layered TMDCs as semiconductor [6-12] has been stimulated by the significant progress in graphene research [13,14]. MoS_2 and WS_2 are widely studied as representative materials because MoS_2 crystals are commercially available for mechanical exfoliation [15-21] and the volatile oxides of MoO_3 and WO_3 can be used as source materials for the chemical vapor deposition (CVD) [22-31]. An advantage of the MoO_3 and WO_3 is that a rugged CVD apparatus can be used to synthesize the monolayer MoS_2 and WS_2. This is because oxide impurities are easily removed from the products due to their high volatility and easy sulfurization. Furthermore, the intriguing electric properties of MoS_2 have attracted many researchers' attention due to the tunable band gap and

direct/indirect transition of the band structure of the monolayer [10,19]. The direct band gap of 1.8 eV is suitable for a wide range of applications such as electronics, photonics, optoelectronics, sensor and bioimaging.

It is desirable to fabricate the p-type MoS_2 (as-grown MoS_2 is the n-type due to S defects) for applications in electronic devices because the next use of MoS_2 devices is based on a p-n junction to fully utilize the excellent electric properties of MoS_2. One of the available dopants to make p-type MoS_2 is Nb. The first demonstration of the Nb-doped MoS_2 was conducted by sulfurization of Mo/Nb/Mo films deposited by e-beam evaporation [32]. However, Mo and Nb were not uniformly distributed in the entire film and the grain size of the Nb-doped MoS_2 was very small (~50 nm), which is much smaller than that of the typical MoS_2 synthesized by CVD (10 - 50 μm). Although Sasaki et al. synthesized the Nb-doped WS_2 from WO_3 and Nb metal [33], a large amount of the oxide impurity (Nb_2O_5) was observed in the film due to the high stability and nonvolatility of Nb_2O_5. In another case, the bulk Nb-doped MoS_2 was made by conventional chemical vapor transport [34], then the monolayer Nb-doped MoS_2 was fabricated by mechanical exfoliation. The mechanical exfoliation is unacceptable for practical applications because the size, position and thickness of MoS_2 cannot be controlled. Chemical doping with thiol molecules was recently reported to tune the electric properties [35-38]. Although the thiol-terminated MoS_2 is desirable as a biosensor and for bioimaging [39], it is unsuitable to control the carrier type and the carrier concentration to make electronic devices because only a fractional carrier was generated from the thiol molecule, and the thiol molecule forms a new trapping state due to the long alkyl chain or benzene moiety [38]. In other words,

tuning of the carrier type and the carrier concentration is difficult and the carrier mobility must be sacrificed as long as the thiol molecule is used. The doping of element is required to achieve a high-performance and multifunctional device with a monolayer MoS_2 as seen in Si technology. Currently, the doping or alloying of MoS_2 with Nb by CVD has not been studied, while the synthesis of the monolayer MoS_2 was reported in many papers [22-31] because most researchers prefer to use the oxide precursor in the CVD due to its easy handling. However, it is impossible to introduce a dopant element (ex. Nb and Ta) with the oxide precursor due to the inevitable inclusion of oxide impurities. Some researchers have synthesized several kinds of alloys such as $Mo_{1-x}W_xS_2$ [40,41] and $MoS_{2(1-x)}Se_{2x}$ [42] with different composition ratios in order to engineer the band gap. Yet, their studies focused on the band gap engineering and did not elucidate the carrier doping.

The present situation must be overcome to realize MoS_2-based electronic devices such as diodes, solar cells and field effect transistors in the future. CVD with all chloride sources is desirable to synthesize the $Mo_{1-x}Nb_xS_2$ thin films as a practical method. Synthesis of MoS_2 and NbS_2 using a chloride source without seed materials [43-45] now makes the doping and alloying realistic.

In this study, we synthesized the $Mo_{1-x}Nb_xS_2$ thin films by CVD using $MoCl_5$ and $NbCl_5$. The Nb concentration was higher than 1% because the Nb concentration would be controlled to the doping level after establishing the method to synthesize the mixed crystals. The separate-flow CVD apparatus make it possible to precisely control the Nb

concentration because the amount of supplied $NbCl_5$ gas can be adjusted by temperature and flow rate. It was found that Nb can be incorporated into the MoS_2 thin film up to 10%.

Experimental details

The $Mo_{1-x}Nb_xS_2$ thin films were synthesized using an atmospheric pressure CVD apparatus with three separate-flow paths as shown in Figure 1. The apparatus was partially modified from the original one [43] to separately introduce the source gases of S, $NbCl_5$, $MoCl_5$ for fabricating $Mo_{1-x}Nb_xS_2$ thin films. The apparatus consisted of a three-zone furnace, an outer quartz tube with an inner diameter of 22 mm, three inner quartz tubes with the inner diameters of 4 mm, three small one-zone furnaces and three source containers. Each zone of the three-zone furnace was called zone A, zone B and zone C from the upper stream. The inner quartz tubes conveying the source gases were called the $MoCl_5$ line, $NbCl_5$ line and S line. The source gases were emitted and mixed in the region between zone A and zone B. We selected $MoCl_5$ as the source material, not MoO_3, which is the common compound for the synthesis of MoS_2 by CVD. It was found in a preliminary experiment that a large amount of Nb_2O_5 was inevitably formed when we used MoO_3, which was confirmed by X-ray diffraction (XRD) (see Fig. 3(a)) and X-ray photoelectron spectroscopy (XPS) (not shown here). It is considered that oxygen contained in the MoO_3 is easily combined with $NbCl_5$ due to the high stability of Nb_2O_5.

The as purchased $MoCl_5$ powder (0.3 g, 99.5 % Kanto Chemical Co., Inc.), $NbCl_5$ (0.3 g, >99.9 %, Kanto Chemical Co., Inc.) and S powder (1.5 g, >99.5 %, Kanto Chemical Co., Inc.) were placed in the corresponding stainless-steel containers. The $MoCl_5$ and $NbCl_5$

were handled in a glove box before sealing the containers because they are air-sensitive. The sealed containers with ultrahigh vacuum ICF (international conflat flange) aluminum gaskets and valves were connected to the CVD apparatus. An air-free atmosphere during the whole process when the chloride sources were handled was very important in order to guarantee the reproducibility. Nothing is formed on the substrate when the nonvolatile oxide covers the surface of the chloride sources. 1 × 1 cm^2 SiO_2(285 nm)/Si substrates cleaned by the RCA method [46] were placed in zone B and zone C. It should be noted that the best position of the substrate was 10 cm from the tip of the inner quartz tube (in the region between zone B and zone C).

The $Mo_{1-x}Nb_xS_2$ thin films were synthesized by the following procedure. The inside atmosphere of the entire system including the quartz tubes and the source containers was pumped off to lower than 10 Pa using a mechanical oil pump. Ultrapure Ar gas (>99.9995 %) then filled the entire apparatus through the S line. The Ar flow (200 sccm) was maintained even while ramping and lowering the temperature to prevent air from intruding into the quartz tube. The $MoCl_5$, $NbCl_5$ and S containers were heated to 140 ºC, 140 - 180 ºC and 240 ºC, respectively. Zones A, B and C were heated to 650 ºC, 1000 ºC and 1000 ºC, respectively, at the ramping rate of 250 ºC/hour. The flow rates of the $MoCl_5$, $NbCl_5$ and S lines were increased to 200 sccm, 200 sccm and 3000 sccm, respectively, to start the reaction. 4% H_2 was used as the carrier gas for the $MoCl_5$ and $NbCl_5$ lines. The reduction reaction of Mo^{5+} and Nb^{5+} into Mo^{4+} and Nb^{4+}, respectively, which takes place on the surface of the substrate, was promoted by the H_2 gas. The Cl atoms were efficiently removed as HCl [43,45]. The exhaust was bubbled through an NaOH solution bubbler

during the CVD. The growth time was defined as the duration of the carrier gas flowing through the $MoCl_5$ and $NbCl_5$ lines. The supply of the $MoCl_5$ and $NbCl_5$ gases was abruptly shut off by closing the main valve to hinder any undesired reaction while lowering the temperature. The three-zone furnace was naturally cooled to room temperature while maintaining the S supply to avoid the oxidation of the thin film until the temperature of zone B reached 350 ºC.

The surface morphology of the $Mo_{1-x}Nb_xS_2$ thin films was observed using an optical microscope (OM) (OLYMPUS BX51). XRD (Rigaku Rint Ultima 2000) was performed to determine the orientation and lattice constants of the grown films using a θ-2θ method in a continuous mode with Cu Kα radiation (λ = 0.154056 nm). The scan step and the scan rate were 0.01º and 5 º/min, respectively. Angular resolution calculated by the formula of $\phi = 2\tan^{-1}(W/2R)$, where W (width of receiving slit) was 0.3 mm and R (length between a sample and receiving slit) was 150 mm, was 0.11º. The chemical composition was estimated by XPS (JEOL JPS-9200, Mg Kα (1286.6 eV)). The emission current density was 10 mA and the spectra were scaled with C1s (285.0 eV). SpecSurf(software) was used for the curve fitting to evaluate the chemical composition ratio. The curve was fitted by Gauss-Lorentz (ratio = 0.7) function and background was subtracted using Shirley method. The carrier type was determined by the measurement of Seebeck coefficient at room temperature. The structure of a selected spot was characterized by Raman spectroscopy (Reinshaw Invia) using a 532-nm excitation laser. The photoluminescence (PL) spectra were obtained by a Raman instrument in the PL mode.

Results and discussion

Independent control of the temperatures and flow rates enabled optimizing the amounts the source gases, which means that the Nb concentration can be tuned by precisely controlling the temperature and flow rate of the $NbCl_5$. While the temperatures of the $MoCl_5$ and S were fixed at 140 ºC and 240 ºC, the temperature of $NbCl_5$ ranged from 140 ºC to 180 ºC. The temperatures of $NbCl_5$ for the synthesis of samples (i), (ii) and (iii) were 140 ºC, 160 ºC and 180 ºC, respectively. The surface morphology was observed by OM as shown in Fig. 2. The number of layers in most regions can be deduced as being more than 20 (mostly bulk) from the interference contrast [31] and the roughness observed by a laser microscope. Although clear triangle domains with a size of 2 μm are seen in the OM images of samples (i) and (ii), domains with a clear shape cannot be seen in one of the sample (iii). In addition, a lot of black particles were formed on sample (iii). The reason why many particles were formed on sample (iii) is discussed later. OM observation suggested that there is a maximum Nb concentration into the MoS_2 thin film without forming particles.

The formation of the $Mo_{1-x}Nb_xS_2$ thin films was confirmed by XRD and XPS. The XRD patterns of all samples and pristine MoS_2 are shown in Fig. 3(a). The peaks marked with red circles were assigned to the (00n) plane of $Mo_{1-x}Nb_xS_2$. It was critical to use a chloride source to synthesize the good quality of $Mo_{1-x}Nb_xS_2$ because a large amount of oxide impurities (Nb_2O_5) was formed when MoO_3 was used as the source material. The XRD pattern of

$Mo_{1-x}Nb_xS_2$ synthesized using MoO_3 and $NbCl_5$ in the preliminary experiment is also shown in Fig. 3(a) (labeled as PE). The oxide formation is consistent with a previous report [33] concerning the Nb-doped WS_2 synthesized using an oxide source (WO_3). The amount of oxide impurities must be decreased because they cause degradation of the electric properties of the $Mo_{1-x}Nb_xS_2$. A small amount of MoO_2 was detected in samples (i) and (iii) even though the inside of the quartz tube was evacuated to lower than 10 Pa before the reaction started and ultrapure Ar was used for the CVD. It is considered that the chloride gas reacted with a small amount of trace oxygen and water in the quartz tube. While a small amount of Nb_2O_5 was detected in sample (ii), a decent amount of Nb_2O_5 was seen in sample (iii). This is probably due to the chance of oxidation of $NbCl_5$ that became higher when the $NbCl_5$ supply increased. It can be concluded that the number of particles increases as the oxide impurities increases as seen in Fig. 2 because they can act as nucleation sites for forming particles. However, it is noteworthy that the amount of oxide impurities was significantly decreased compared to the one synthesized using an oxide source.

The peaks assigned to (002) of $Mo_{1-x}Nb_xS_2$ are slightly shifted from the original position of MoS_2 as shown in Fig. 3(b) (extracted from Fig. 3(a)). The peak centers of the pristine MoS_2, samples (i), (ii) and (iii) are 14.39º, 14.41º, 14.43º and 14.46º, respectively. Unfortunately, the greatest difference of 2θ is smaller than angular resolution (0.11º), However, we notice that there is no splitting at (002) peaks in XRD. The films consisted of well-defined triangular domains with the size of ~2 μm (Fig. 2). This size was much greater than the thickness of the film (> 20 nm), which was estimated from the greatest roughness observed by laser microscope. Therefore, it is reasonable to assume the size of the

crystallites in the (002) direction was the thickness of the film. By using this assumption with the Scherrer equation $\tau = K\lambda / \beta \cos \theta$, where τ = 20 nm, K~0.9 (shape factor), λ = 0.154056 nm (X-ray wavelength), β is FWHM of XRD peak, θ is the diffraction angle (~7.2°). Then β = 0.007° and far below the angular resolution of the instrument (0.11°). Therefore, our XRD would detect the difference of interlayer distances of MoS_2 (0.6155 nm, (002) diffraction at 14.38°) and NbS_2 (0.5960 nm, (003) diffraction at 14.85°), if they formed different domains. It is noteworthy that Nb concentrations were deduced as 6 % for (i), 11 % for (ii) and 17 % for (iii) if Vegard's law is applicable.

The Nb concentration was evaluated by XPS based on the peak area ratio of the Mo^{4+} $3d_{5/2}$, Nb^{4+} $3d_{5/2}$ and S^{2-} $2p_{3/2}$ peaks and their sensitivity factors. Figure 4 shows the XPS spectra of all samples. The chemical ratios of samples (i), (ii) and (iii) were estimated as Mo^{4+}:Nb^{4+}:S^{2-} = 0.96:0.04:2.0, 0.90:0.10:1.95 and 0.37:0.63:2.05, respectively. The Nb^{4+} concentrations of samples (i) and (ii) are reasonable when considering the XRD results. However, the Nb^{4+} concentration of sample (iii) evaluated from the XPS is much higher than that expected from the XRD results. This is probably because there are amorphous regions with a Nb-rich composition and Nb^{5+} originated from Nb_2O_5. The lack of triangle domains in Fig. 2(c) also implies the poor crystallinity of sample (iii). Nb^{5+} in sample (iii) is attributed to the Nb_2O_5 when the XRD result is taken into account. By combining the XPS result with the well-defined triangular domains shown in Fig. 2, it became clear that the Nb concentration can be increased to 10% without forming particles by controlling the temperature of the $NbCl_5$. The Seebeck coefficient was measured to determine the carrier

type of the $Mo_{1-x}Nb_xS_2$ thin films. It was evaluated as +44.2 μV/K at 20 °C, which indicates that the $Mo_{1-x}Nb_xS_2$ was p-type.

There are three possibilities of how the Nb atoms were incorporated into the $Mo_{1-x}Nb_xS_2$ thin films: (a) single layer alloys by replacing Mo with Nb, (b) the MoS_2 domain and NbS_2 domain were separately formed, and (c) the MoS_2 layer and NbS_2 layer were randomly stacked. The result of the XRD patterns excludes the possibility of (b). Raman and PL spectra were obtained to determine which of (a) or (c) is real in our sample.

Figure 5 shows the Raman spectra of all samples. The Raman spectra of the pristine MoS_2 and 3R-NbS_2 are also shown for comparison. The in-plane vibrational modes of MoS_2 and NbS_2 are called E_{2g} and E_2, respectively, and the out-of-plane vibrational mode of MoS_2 and NbS_2 are called A_{1g} and A_1, respectively, as shown in Fig. 5. All the spectra, except 3R-NbS_2, were normalized with the A_{1g} (Mo-S) peak in order to easily compare the ratio of the peak intensities A_{1g} (Mo-S) and E_2 (Nb-S), and the spectrum of 3R-NbS_2 was scaled to clearly see the position of the E_2 peak. When the Nb concentration is low (sample (i)), the spectrum is similar to that of the pristine MoS_2 film. When the Nb concentration reaches 10% that was evaluated by XPS, the vibrational modes (E_2) related to Nb-S appeared. It should be noted that although there are four original peaks (E_1, E_2, A_1 and A_2) for the pristine 3R-NbS_2, only the E_2 peak is distinguishable for $Mo_{1-x}Nb_xS_2$ because the intensity of A_2 and E_1 is low and the position of A_1 is overlapped with one of the MoS_2 peaks. The broad band at 100 - 200 cm^{-1} is due to impurities or defects which are always found even in the case of a synthetic NbS_2 bulk single crystal [47]. The intensity of the E_2

mode gradually becomes stronger as the Nb concentration increases. The gradual increase in the intensity was consistent with a previous study of $MoS_{2(1-x)}Se_{2x}$ [42] whose S and Se were homogeneously distributed in the entire films. Such a transition of the vibrational mode was also observed in the $Si_{1-x}Ge_x$ alloy [48]. The peak position is independent on the Nb concentration for $Mo_{1-x}Nb_xS_2$, while a peak shift was observed in the previous studies of $MoS_{2(1-x)}Se_{2x}$ and $Si_{1-x}Ge_x$. The strength of the Mo-S bonding was not significantly affected by the Nb concentration since the mass of Nb does not significantly differ from that of Mo. This is the reason why the peak intensity changed as the Nb concentration changed, while the peak position did not change. Hence, the Raman spectra does not exclude the possibility of uniform distribution of Nb atoms in the $Mo_{1-x}Nb_xS_2$ thin films.

The PL spectra were measured in a monolayer region for samples (i) - (iii) to prove the formation of the $Mo_{1-x}Nb_xS_2$ as shown in Fig. 6. The pristine MoS_2 thin film has an intense peak at 655 nm, which is a unique optical property of MoS_2 due to the reduced dielectric screening and enhanced Coulomb interaction [49-51]. The small peak at 605 nm is due to the spin split valence bands at the K-valley (B exciton) [19, 23, 49]. As Nb was incorporated into the MoS_2, two noticeable features were observed. One of them is that the wavelength of PL from the B exciton was longer than that of the pristine MoS_2 (635 nm). This can be explained by assuming many body effects induced by an increase in the free carrier [52]. The other thing is that the (655 nm) peak due to A excitons disappeared and a new peak appeared at 680 nm. This can be interpreted as the major PL origin was changed from A excitons to trions. According to Refs. 46 and 47, the PL emitted by A excitons strongly depends on the carrier concentration while the one by trions is independent of the

carrier concentration. Taking this theory into consideration, it is considered that hole-hole-electron trions were generated by light irradiation in our $Mo_{1-x}Nb_xS_2$ thin films while electron-electron-hole trions have been mainly studied in the literature [49,50]. When the electron concentration in MoS_2 reaches 6×10^{12} cm^{-2}, the exciton peak disappeared in the previous study and only the trion peak was detected. Assuming that all the Nb atoms were ionized in the $Mo_{1-x}Nb_xS_2$, the hole concentration of sample (i) (lowest concentration) can be calculated as 2.3×10^{13} cm^{-2}, which exceeds the minimum concentration that eliminates the A exciton peak [49]. Disappearance of the trion peak for sample (iii) is probably due to the poor crystallinity and oxide impurities, which is not surprising because the PL spectra was influenced by the sample condition even though the measurement condition was the same [50]. The PL spectra indicate that the possibility of (c) is eliminated, which means that single layer alloys were formed.

In this research, p-type behavior of the $Mo_{1-x}Nb_xS_2$ was confirmed by the measurement of Seebeck coefficient as well as the Nb concentration was increased up to 10% without forming particles. For such a high impurity level, it should be called as alloying or solid solution rather than doping. At a lower concentration (1 - 100 ppm), it is impossible to detect the dopant element by XRD, XPS and Raman spectroscopy. However, our approach can be applied to make the Nb-doped MoS_2 (impurity level is lower than 1%) by precisely controlling the amount of the supplied $NbCl_5$ vapor. Additionally, our method can be utilized for any combination of TMDCs if the corresponding volatile chloride is available.

Conclusions

We have demonstrated that $Mo_{1-x}Nb_xS_2$ thin films were synthesized using a separate-flow CVD apparatus. The chloride source is key to incorporate Nb into MoS_2 to exclude the oxide impurities. The Nb concentration can be increased to 10% by changing the amount of the $NbCl_5$ supply for maintaining the crystallinity, which was confirmed by XRD, XPS, Raman spectroscopy and PL measurement. p-type behavior was confirmed by the measurement of the Seebeck coefficient. We believe that our demonstration encourages researchers to deeply study the doping and develop more practical devices based on the p-n junction and valleytronics.

Acknowledgements

Instrumental analysis was supported by the Nanotechnology Platform at Hokkaido University by METI, Japan.

Funding

This research was partly supported from KAKENHI 2612050205 and 15K1411405.

References

[1] P.R. Wentrcek, H. Wise, Hydrodesulfurization activity and defect structure of Co-Mo sulfide catalyst, J. Catal. 51 (1978) 80-85. DOI:10.1016/0021-9517(78)90240-3

[2] L.E. Pope, T. R. Jervis, M. Nastasi, Effects of laser processing and doping on the lubrication and chemical properties of thin MoS_2 films, Surf. Coat. Technol. 42 (1990) 217-225. DOI:10.1016/0257-8972(90)90154-5

[3] S.K. Behal, R.R. Chianelli, B.H. Kear, Edge plane segregation in cobalt-doped MoS_2 crystals, Mater. Lett. 3 (1985) 381-384. DOI:10.1016/0167-577X(85)90082-5

[4] A. Koma, K. Sunouchi, T. Miyajima, Fabrication and characterization of heterostructures with subnanometer thickness, Microelectron. Eng. 2, (1984) 129-136. DOI:org/10.1016/0167-9317(84)90057-1

[5] T. Shimada, FS. Ohuchi, A. Koma, Polytypes and charge-density waves of ultrathin TaS_2 films grown by van der Waals epitaxy, Surface Science 291, (1993) 57-66. DOI:org/10.1016/0039-6028(93)91476-6

[6] J.A. Wilson, A.D. Yoffe, The transition metal dichalcogenides discussion and interpretation of the observed optical, electrical and structural properties, Adv. Phys. 18 (1969) 195-335. DOI:10.1080/00018736900101307

[7] K.S. Novoselov, D. Jiang, F. Schedin, T. J. Booth, V.V. Khotkevich, S.V. Morozov, A.K. Geim, Two-dimensional atomic crystals, Proc. Nat. Acad. Sci. 102 (2005) 10451-10453. DOI:10.1073/pnas.0502848102

[8] S. Das, H.Y. Chen, A.V. Penumatcha, J. Appenzeller, High performance multilayer MoS_2 transistors with scandium contacts, Nano Lett. 13 (2013) 100-105. DOI:10.1021/nl303583v

[9] W. Guo, X. Liu, 2D materials. Metallic when narrow, Nature Nanotech. 9 (2014) 413-414. DOI:10.1038/nnano.2014.106

[10] B. Radisavljevic, A. Radenovic, J. Brivio, V. Giacometti, A. Kis, Single-layer MoS_2 transistors, Nature Nanotech. 6 (2011) 147-150. DOI:10.1038/nnano.2010.279

[11] J. Pu, Y. Yomogida, K.K. Liu, L.J. Li, Y. Iwasa, T. Takenobu, Highly flexible MoS_2 thin-film transistors with ion gel dielectrics, Nano Lett. 12 (2012) 4013-4017. DOI:10.1021/nl301335q

[12] R. Lv, J. Robinson, R.E. Schaak, D. Sun, Y. Sun, T.E. Mallouk, M. Terrones, Transition metal dichalcogenides and beyond: synthesis, properties, and applications of single- and few-layer nanosheets, Acc. Chem. Res. 48 (2015) 56-64. DOI:10.1021/acs.accounts.5b00076

[13] K.S. Novoselov, V.I. Fal'ko, L. Colomno, P.R. Gellert, M.G. Schwab, K. Kim, A roadmap for graphene, Nature 490 (2012) 192-200. DOI:10.1038/nature11458

[14] X. Li, W. Cai, J. An, S. Kim, J. Nah, D.Yang, R. Piner, A. Velamakanni, I. Jung, E. Tutuc, S.K. Banerjee, L. Colombo, R.S. Ruoff, Large-area synthesis of high-quality and uniform graphene films on copper foils, Science, 324 (2009) 1312-1314. DOI:10.1126/science.1171245

[15] Y. Wang, C. Cong, C. Qiu, T. Yu, Raman Spectroscopy Study of Lattice Vibration and Crystallographic Orientation of Monolayer MoS_2 under Uniaxial Strain, Small 17 (2013) 2857-2861. DOI:10.1002/smll.201202876

[16] R. Addou, S. McDonnell, D. Barrera, Z. Guo, A. Azcatl, J. Wang, H. Zhu, C.L. Hinkle, M. Quevedo-Lopez, H.N. Alshareef, L. Colombo, J.W. Hsu, R.M. Wallace, Impurities and electronic property variations of natural MoS_2 crystal surfaces, ACS NANO 9 (2015) 9124-9133. DOI:10.1021/acsnano.5b03309

[17] D. Lembke, A. Kis, Breakdown of High-Performance Monolayer MoS_2 transistors ACS NANO 6 (2012) 10070-10075. DOI:10.1021/nn303772b

[18] H. Li, Q. Zhang, C. Chong, R. Yap, B.K. Tay, T. Hang, T. Edwin, A. Olivier, D. Baillargeat, From bulk to monolayer MoS_2: evolution of Raman scattering Adv. Funct. Mater. 22 (2012) 1385-1390. DOI:10.1002/adfm.201102111

[19] A. Splendiani, L. Sun, Y. Zhang, T. Li, J. Kim, C.Y. Chim, G. Galli, F. Wang, Emerging photoluminescence in monolayer MoS_2, Nano Lett. 10 (2010) 1271-1275. DOI:10.1021/nl903868w

[20] S. Balendhran, J.Z. Ou, M. Bhaskaran, S. Sriram, S. Ippolito, Z. Vasic, E. Kats, S. Bhargava, S. Zhuiykov, K. Kalantar-zadeh, Atomically thin layers of MoS_2 *via* a two step thermal evaporation-exfoliation method, Nanoscale, 4 (2012) 461-466. DOI:10.1039/C1NR10803D

[21] S.L. Li, H. Miyazaki, H. Song, H. Kuramochi, S. Nakaharai, K. Tsukagoshi, Quantitative Raman spectrum and reliable thickness identification for atomic layers on insulating substrate, ACS NANO 6 (2012) 7381-7388. DOI:10.1021/nn3025173

[22] Y.H. Lee, X.Q. Zhang, W. Zhang, M.T. Chang, C.T. Lin, K.D. Chang, Y.C. Yu, J.T. W. Wang, C.S. Chang, L. Li, T.W. Lin, Synthesis of large-area MoS_2 atomic layers with chemical vapor deposition, Adv. Mater. 24 (2012) 2320-2325. DOI:10.1002/adma.201104798

[23] S. Wang, Y. Rong, Y. Fan, M. Pacios, H. Bhaskaran, K. He, J.H. Warner, Shape evolution of monolayer MoS_2 crystals grown by chemical vapor deposition, Chem. Mater. 26 (2014) 6371-6379. DOI:10.1021/cm5025662

[24] J. Zhang, H. Yu, H.W. Chen, X. Tian, D. Cheng, M. Liu, M.G. Xie, W. Yang, R. Yang, X. Bai, D. Shi, G. Zhang, Scalable growth of high-quality polycrystalline MoS_2 monolayer on SiO_2 with tunable grain sized, ACS NANO 8 (2014) 6024-6030. DOI:10.1021/nn5020819

[25] H. Schmidt, S. Wang, L. Chu, M. Toh, R. Kumar, W. Zhao, A.H.C. Neto, J. Martin, S. Adam, B. Ozyilmaz, G. Eda, Transport properties of monolayer MoS_2 grown by chemical vapor deposition, Nano Lett. 14 (2014) 1909-1913. DOI:10.1021/nl4046922

[26] W. Park, J. Baik, T.Y. Kim, K. Cho, K.W.K. Hong, H.J. Shin, T. Lee, Photoelectron spectroscopic imaging and device applications of large-area patternable single-layer MoS_2

synthesized by chemical vapor deposition, ACS NANO 8 (2014) 4961-4968. DOI:10.1021/nn501019g

[27] W. Zhu, T. Low, Y. Lee, H. Wang, D.B. Farmer, J. Kong, F. Xia, P. Avouris, Electronic transport and device prospects of monolayer molybdenum disulphide grown by chemical vapour deposition, Nature Commun. 5 (2014) 4087/1-4087/8. DOI:10.1038/ncomms4087

[28] S. Kim, V.K. Sangwan, D. Jariwala, J.D. Wood, S. Park, K.S. Chen, F. Shi, F. Ruiz-Zepeda, A. Ponce, M. Jose-Yacaman, V.P. Dravid, T.J. Marks, M.C. Hersam, L.J. Lauhon, Influence of stoichiometry on the optical and electrical properties of chemical vapor deposition derived MoS_2, ACS NANO 8 (2014) 10551-10558. DOI:10.1021/nn503988x

[29] A.M. van der Zande, P.Y. Huang, D.A. Chenet, T.C. Berkelbach, Y. You, G.H. Lee, T.F. Heinz, D.R. Reichman, D.A. Muller, J.C. Hone, Grains and grain boundaries in highly crystalline monolayer molybdenum disulphide, Nature Mater. 12 (2013) 554-561. DOI:10.1038/nmat3633

[30] Y. Yoo, Z.P. Degregorio, J.E. Johns, Seed crystal homogeneity controls lateral and vertical heteroepitaxy of monolayer MoS_2 and WS_2, J. Am. Chem. Soc. 137 (2015) 14281-14287. DOI:10.1021/jacs.5b06643

[31] T. Yanase, S. Watanabe, M. Weng, T. Nagahama, T. Shimada, Chemical vapor deposition of MoS_2: insight into the growth mechanism by separated gas flow experiments, J. Nanosci. Nanotech. 16 (2016) 3223-3227. DOI:10.1166/jnn.2016.12313

[32] M.R. Laskar, D.N. Nath, L. Ma, E.W. Lee II, C.H. Lee, T. Kent, Z. Yang, R. Mishra, M.A. Roldan, J.C. Idrobo, S.T. Pantelides, S.J. Pennycook, R.C. Myers, Y. Wu, S. Rajan, p-type doping of MoS_2 thin films using Nb, Appl. Phys. Lett. 104 (2014) 092104/1-092104/4. DOI:10.1063/1.4867197

[33] S. Sasaki, Y. Kobayashi, Z. Liu, K. Suenaga, Y. Maniwa, Y. Miyauchi, Y. Miyata, Growth and optical properties of Nb-doped WS_2 monolayers, Appl. Phys. Exp. 9 (2016) 071201/1-071201/4. DOI:10.7567/APEX.9.071201

[34] J. Suh, T.E. Park, D.Y. Lin, D. Fu, J. Park, H.L. Jung, Y. Chen, C. Ko, C. Jang, Y. Sun, R. Sinclair, J. Chang, S. Tongay, J. Wu, Doping against the native properties of MoS_2: degenerate hole doping by cation substitution, NANO Lett. 14 (2014) 6976-6982. DOI:10.1021/nl503251h

[35] S. Mouri, Y. Miyauchi, K. Matsuda, Chemical doping modulation of nonlinear photoluminescence properties in monolayer MoS_2, Appl. Phys. Exp. 9 (2016) 055202/1-055202/4. DOI:10.7567/APEX.9.055202

[36] Q. Ding, K.J. Czech, Y. Zhao, J. Zhai, R.J. Hamers, J.C. Wright, S. Jin, Basal-plane ligand functionalization on semiconducting 2H-MoS_2 monolayers, Appl. Mat. Interfaces 9 (2017) 12734–12742. DOI:10.1021/acsami.7b01262

[37] D.M. Sim, M. Kim, S. Yin, M.J. Choi, J. Choi, S. Yoo, Y.S. Jung, Controlled doping of vacancy-containing few-layer MoS_2 via highly stable thiol-based molecular chemisorption, ACS Nano 9 (2015) 12115-12123. DOI:10.1021/acsnano.5b05173

[38] K. Cho, M. Min, T.Y. Kim, H. Jeong, J. Pak, J.K. Kim, J. Jang, S.J. Yun, Y.H. Lee, W.K. Hong, T. Lee, Electrical and optical characterization of MoS_2 with sulfur vacancy passivation by treatment with alkanethiol molecules, ACS Nano 9 (2015) 8044-8053. DOI:10.1021/acsnano.5b04400

[39] X.Li, J. Shan, W. Zhang, S. Su, L. Yuwen, L. Wang, Recent advances in synthesis and biomedical applications of two dimensional transition metal dichalcogenide nanosheet, Small 13 (2017) 1602660. DOI:10.1002/smll.201602660

[40] Z. Wang, P. Liu, Y. Ito, S. Ning, Y. Tan, T. Fujita, A. Hirata, M. Chen, Chemical vapor deposition of monolayer $Mo_{1-x}W_xS_2$ crystals with tunable band gaps, Sci. Rep. 6 (2016) 21536/1-21536/9. DOI:10.1038/srep21536

[41] Y. Chen, W. Wen, Y. Zhu, N. Mao, Q. Feng, M. Zhang, H.P. Hsu, J. Zhang, Y.S. Huang, L. Xie, Temperature-dependent photoluminescence emission and Raman scattering from $Mo_{1-x}W_x$ S_2 monolayers, Nanotech. 27 (2016) 445705/1-445705/6. DOI:10.1088/0957-4484/27/44/445705

[42] H. Li, Q. Zhang, X. Duan, X. Wu, X. Fan, X. Zhu, X. Zhuang, W. Hu, H. Zhou, A. Pan, X. Duan, Lateral growth of composition graded atomic layer $MoS_{2(1-x)}Se_{2x}$ nanosheets, J. Am. Chem. Soc. 137 (2015) 5284–5287. DOI:10.1021/jacs.5b01594

[43] T. Yanase, S. Watanabe, M. Weng, M. Wakeshima, Y. Hinatsu, T. Nagahama, T. Shimada, Chemical vapor deposition of NbS_2 from a chloride source with H_2 Flow: orientation control of ultrathin crystals directly grown on SiO_2/Si substrate and charge

density wave transition, Cryst. Growth Des. 16 (2016) 4467-4472. DOI:10.1021/acs.cgd.6b00601

[44] Y. Yu, C. Li, Y. Liu, L. Su, Y. Zhang, L. Cao, Controlled scalable synthesis of uniform, high-quality monolayer and few-layer MoS_2 films, Sci. Rep. 3 (2013) 1866/1-1866/6. DOI:10.1038/srep01866

[45] C.C. Huang, F.A. Saab, Y. Wang, J.Y. Ou, J.C. Walker, S. Wang, B. Gholipour, R.E. Simpson, D.W. Hewak, Scalable high-mobility MoS_2 thin films fabricated by an atmospheric pressure chemical vapor deposition process at ambient temperature, Nanoscale 6 (2014) 12792-12797. DOI:10.1039/C4NR04228J

[46] K. Kern, The Evolution of silicon wafer cleaning technology, J. Electrochem. Soc. 137 (1990) 1887-1892. DOI:10.1149/1.2086825

[47] W.G. McMullan, J.C. Irwin, Raman scattering from 2*H* and 3*R*-NbS_2, Solid State Commun. 45 (1983) 557-560. DOI:10.1016/0038-1098(83)90426-X

[48] M.I. Alonso, K. Winer, Raman spectra of *c*-$Si_{1-x}Ge_x$ alloys, Phys. Rev. B 39 (1989) 10056-10062. DOI:org/10.1103/PhysRevB.39.10056

[49] K.F. Mak, K. He, C. Lee, G. H. Lee, J. Hone, T.F. Heinz, J. Shan, Tightly bound trions in monolayer MoS_2, Nature Mat. 12 (2013) 207-211. DOI:10.1038/nmat3505

[50] H.S. Lee, M.S. Kim, H. Kim, Y.H. Lee, Identifying multiexcitons in MoS_2 monolayers at room temperature, Phys. Rev. B 93 (2016) 140409/1-140409/6. DOI:10.1103/PhysRevB.93.140409

[51] F.C. Simon, T.M. Gay, D. Lagarde, G. Wang, C. Robert, P. Renucci, B. Urbaszek, X. Marie, Well separated trion and neutral excitons on superacid treated MoS_2 monolayers, Appl. Phys. Lett. 108 (2016) 108 251106/1-251106/4. DOI:10.1063/1.4954837

[52] Y. Park, S.W. Han, C.C.S. Chan, B.P.L. Reid, R.A. Taylor, N. Kim, Y. Jo, H. Im, K.S. Kim, Interplay between many body effects and coulomb screening in the optical bandgap of atomically thin MoS_2, Nanoscale 9 (2017) 10647-10652. DOI:10.1039/C7NR01834G

Figure captions

Fig. 1: Schematic illustration of three separate-flow CVD apparatus. Source gases of S, $NbCl_5$ and $MoCl_5$ can be separately introduced into the reaction region for controlling the Nb concentration.

Fig.2: Optical microscopic images of $Mo_{1-x}Nb_xS_2$ for samples (i), (ii) and (iii).

Fig. 3: (a) XRD patterns of the pristine MoS_2 and all samples. The (00n) peaks (marked with red circle) were assigned to the $Mo_{1-x}Nb_xS_2$. The XRD pattern labeled as PE shows the $Mo_{1-x}Nb_xS_2$ synthesized with MoO_3 and $NbCl_5$ as the source materials. (b) Extraction of XRD patterns from 14º to 15º. No peak splitting shows that two separate domains of MoS_2 and NbS_2 were not formed.

Fig. 4: XPS spectra of all the samples. The chemical ratios were calculated using Mo^{4+} $3d_{5/2}$, Nb^{4+} $3d_{5/2}$ and S^{2-} $2p_{3/2}$ as Mo^{4+}:Nb^{4+}:S^{2-}=0.96:0.04:2.0 for (i), 0.90:0.10:1.95 for (ii) and 0.37:0.63:2.05 for (iii). Nb can be incorporated into MoS_2 up to 10% without oxide impurities.

Fig. 5: Raman spectra of all the samples. The transformation of the spectra is due to the Nb incorporation. Spectra of the pristine MoS_2 and NbS_2 are also shown for comparison.

Fig. 6: PL spectra of all samples. Spectra of the pristine MoS_2 are also shown for comparison. PL from the A excitons disappeared due to the alloying with Nb.

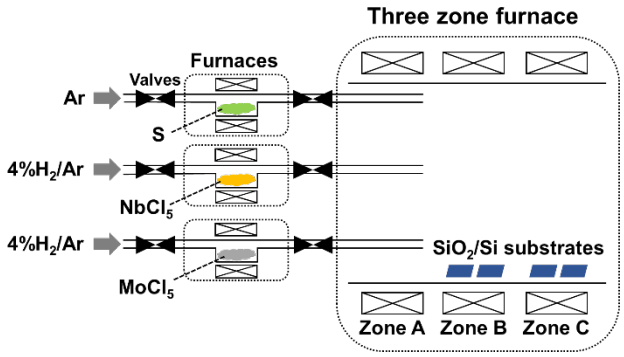

Fig. 1 (color online)

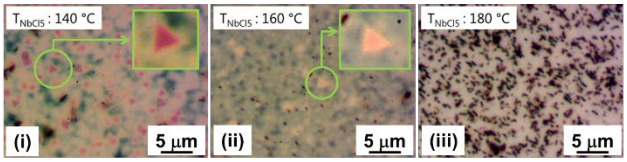

Fig. 2 (color online)

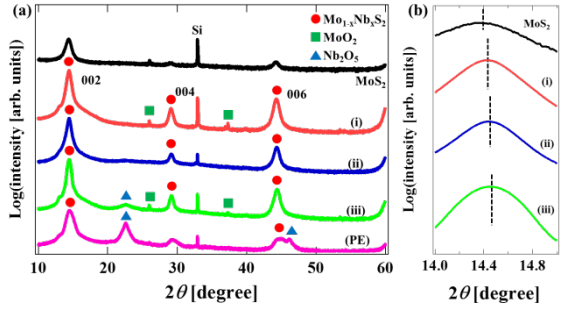

Fig. 3 (color online)

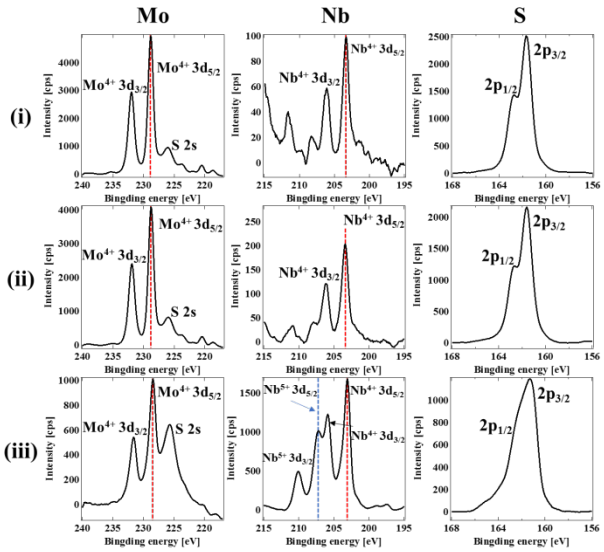

Fig. 4 (color online)

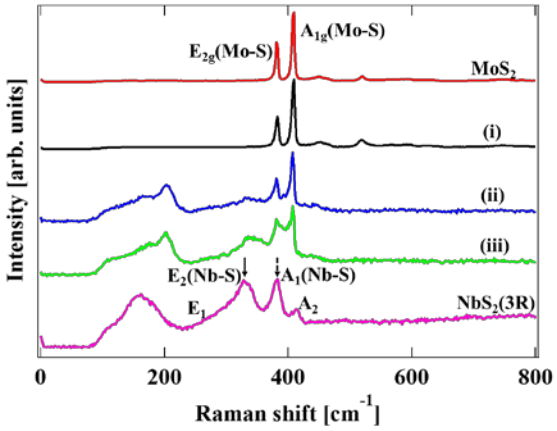

Fig. 5 (color online)

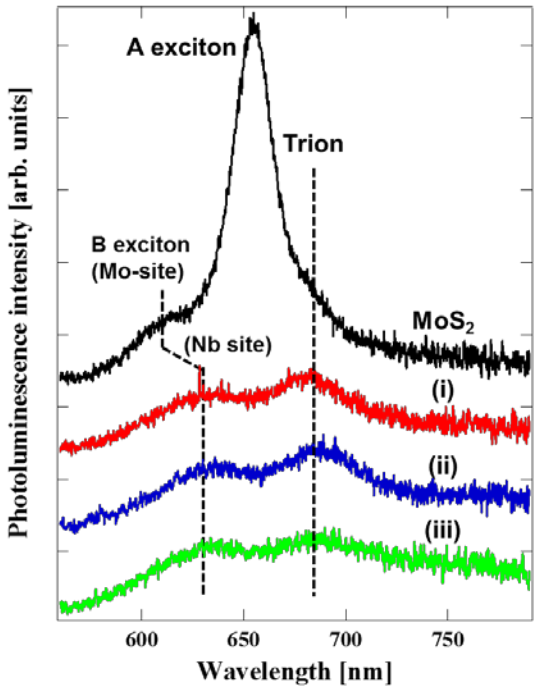

Fig. 6 (color online)